ELSEVIER

Polymer 42 (2001) 1183–1200

polymer

www.elsevier.nl/locate/polymer

Morphology and mechanical properties of swollen gels and dry gel films of poly(vinyl alcohol) prepared by crystallization from solutions under simultaneous biaxially stretching

Y. Bin, Y. Tanabe, C. Nakabayashi, H. Kurosu, M. Matsuo*

Department of Textile and Apparel Science, Faculty of Human Life and Environment, Nara Women's University, Nara 630-8263, Japan

Received 4 November 1999; received in revised form 9 March 2000; accepted 7 June 2000

Abstract

Simultaneous biaxial stretching was carried out by using poly(vinyl alcohol) (PVA) gel films which were prepared by crystallization from solutions in dimethyl sulfoxide (Me_2SO) and water (H_2O) mixtures. The Me_2SO/H_2O composition was set to be 70:30. The maximum biaxially draw ratio, 3×3, is much lower than 8.7×8.7 of ultra-high-molecular-weight polyethylene (UHMWPE) dry gel films. Even so, Young's modulus of the PVA film was almost equal to that of the UHMWPE. To address this problem, theoretical analysis was carried out using a three-dimensional model, in which the oriented crystalline layers are surrounded by an anisotropic amorphous phase and the strains of the two phases at the boundary are identical. Young's modulus was calculated by using the generalized orientation factors of crystallites and amorphous chain segments estimated from the orientation functions of crystallites and amorphous chain segments. The experimental values were lower than the calculated one. Such a disagreement between the experimental and calculated values was discussed in relation to the morphology estimated by high-resolution solid state ^{13}C NMR spectroscopy. Furthermore, the ultimate value of Young's modulus was estimated theoretically by assuming an ideal simultaneous biaxially stretched film with 100% crystallinity and the perfect orientation of the *c*-axes parallel to the film surface. The predicted value at absolute temperature was less than 13.5 GPa, suggesting the impossibility to produce high-modulus and high-strength PVA sheets. Incidentally, the stress–strain curves repeated up to 40 times of swollen gels with large amount of solvents >80% passed through the same hysteresis route indicating rubber elasticity. Such an interesting phenomenon was investigated in relation to crystallization by small angle light scattering under Hv polarization condition and X-ray diffraction.

Keywords: Simultaneous biaxial stretching; Orientation functions of crystallites; Rubber elasticity

1. Introduction

It is well-known that the effective drawability of ultra-high-molecular-weight polyethylene (UHMWPE) prepared by the gel deformation method is dramatically enhanced using specimens spun or cast from semi-dilute solutions to form macroscopic gels [1–5]. The dry gel films of UHMWPE (molecular weight of 6×10^6) could be elongated up to 400 times and Young's modulus reached 216 GPa [6,7], when the gels were prepared from solutions with optimum concentration. The value is close to the ultimate value corresponding to the crystal lattice modulus (220–235 GPa) along the chain direction measured by X-ray diffraction at room temperature [6,8], while the crystal lattice modulus at −155°C close to the glass transition temperatures is reported to be 254 GPa [9], indicating that the crystal lattice modulus increases when the local motion of the chain segments was frozen.

With regard to biaxially stretched films, a number of papers have been reported for the deformation mechanism of poly(ethylene terephthalate) [10], polypropylene [11] and poly(vinyl alcohol) films [12]. Among them, UHMWPE dry gel films with the greatest drawability under uniaxial elongation also causes significant effect on the biaxial one. The biaxial elongation for UHMWPE was first done by Miyasaka et al. [13–15]. They studied the development of fibrillar texture and the mechanical properties of UHMWPE dry gel films. Further estimations have been done for the deformation mechanism and mechanical properties by Gerrits et al. [16–18] in terms of crystal plasticity on the basis of the planner orientation of crystallites and by Bastiaansen et al. [19] in terms of experimental and theoretical aspects. They pointed out that Young's modulus and tensile strength cannot be improved in contrast to those of

* Corresponding author. Tel.: +81-742-20-3462; fax: +81-742-20-3462/3499.

E-mail address: m-matsuo@cc.nara-wu.ac.jp (M. Matsuo).

0032-3861/01/$ - see front matter
PII: S0032-3861(00)00423-7

uniaxially drawn tapes. To give more quantitative estimation for the simultaneous biaxially stretching mechanism of UHMWPE dry gel films, Nakashima et al. [20] studied the morphology and mechanical properties of the films in relation to the optimum concentration assuring the greatest significant drawability. In doing so, the deformation mechanism was analyzed by the orientation distribution function of crystallites which can be estimated by the orientation distribution functions of the reciprocal lattice vectors of the crystal planes around the film normal direction by using the method of Roe and Krigbaum [21–23].

For poly(vinyl alcohol) (PVA) films, the biaxially stretching was done by Hibi et al. for water cast films [12]. They proposed one of the refined methods to connect Young's modulus and the fourth-order orientation factors of the crystallites and amorphous chain segments. Unfortunately, the power of their X-ray instrument was too weak to obtain the diffraction intensity from several crystal planes. They postulate the fourth-order orientation factors of crystallites on the basis of the two reflections of the (110) and $(1\bar{1}0)$ planes by assuming an inversely superposed Gaussian function.

To study the morphology and mechanical properties of dry and swollen PVA gels, this paper concentrates mainly on two viewpoints. One is the theoretical calculation of Young's modulus on the basis of the generalized orientation factors of crystallites estimated from the orientation distribution functions of the reciprocal lattice vectors of the seven crystal planes to avoid the ambiguous assumption by Hibi et al. [12]. By using this method, the orientation distribution functions of the crystallographic principle axes, *a*-, *b*-, and *c*-axes of PVA crystallites were proposed, because of the difficulty in the peak separation of overlapped X-ray reflection from the individual crystal planes. With a simple application, an ultimate value of Young's modulus of simultaneous biaxially stretched film was postulated in the ideal case with 100% crystallinity and perfect orientation of the *c*-axes parallel to the film surface. The other is the rubber elasticity of PVA gels containing a large amount of solvent. The rubber elasticity of the gels prepared by quenching solutions has never been reported for polyethylene and polypropylene gels. Such interesting properties are discussed in relation to the morphology of the swollen gels by using small angle light scattering under Hv polarization condition and X-ray diffraction.

2. Experimental

2.1. Sample preparation

PVA powder with polymerization of 2000 and 98% hydrolysis was used as test specimens. The PVA gels were prepared by crystallization from semi-dilute solutions in the dimethyl sulfoxide (Me_2SO) and water (H_2O) mixtures. The Me_2SO/H_2O composition was set to be 70:30 (v/v) assuring the high drawability of PVA films in accordance with a report by Cha et al. [24]. Here, we must emphasize that this composition also ensures very slow evaporation of solvent from the swollen gels. Through trial and error, 10 g/100 ml was found to be the best concentration to ensure the greatest significant biaxially drawing. The solutions were prepared by heating the well-blended polymer/solvent mixture at 105°C for 40 min. The hot homogenized solution was quenched by pouring it into an aluminum tray controlled at 25°C or −30°C, thus generating a gel.

The gel film containing solvent was cut into strips of $90 \times 90\ mm^2$. The specimen was elongated biaxially up to the desired ratio by using an Iwamoto biaxial stretcher at room temperature. After stretching, the sample fixed in the biaxial stretcher was air-dried at room temperature to evaporate the solvent. The resultant dry gel film was removed from the stretcher. In this process, any shrinkage did not occur. The draw ratio was determined in the usual way by measuring the displacement of ink marks placed 5×5 mm apart on the specimen prior to drawing. Another experiment was carried out to study the stress–relaxation behavior of the wet gels on the basis of hysteresis curves. In doing so, the repeated experiment of elongation and recovery was done up to 40 times with the same speed of $5\ mm\ min^{-1}$.

2.2. Sample characterization

The density of the films was measured by a pycnometer with *p*-xylene and carbon tetrachloride as the medium. Since the density was very dependent on the presence of residual solvent in the film, great care was taken to remove the solvent. Namely, samples were cut into fragments and subsequently vacuum-dried for 3 days at 60°C prior to measuring the density. The dried fragments were immersed in *p*-xylene–carbon tetrachloride for a day to promote the penetration of the solvents into voids of the sample and then the density measurements were carried out. Crystallinity was calculated by assuming the densities of the crystalline and amorphous phases to be 1.345 and $1.269\ g\ cm^{-3}$, respectively [25].

To measure Young's modulus and tensile strength, the specimens were elongated at 20°C with an Instron tester at the cross head speed of $20\ mm\ min^{-1}$. The initial dimensions of the samples were: length 40 mm and width 4 mm.

The complex dynamic tensile modulus was measured at 10 Hz over the temperature range from −100 to 50°C for wet gels and over the temperature range from −150 to 300°C for dry gel films by using a visco-elastic spectrometer (VES-F) obtained from Iwamoto Machine Co. Ltd. The length of the specimen between the jaws was 40 mm and the width was about 1.5 mm. During measurements, the specimen was subjected to a static tensile strain in order to place the sample in tension during the axial sinusoidal oscillation. The complex dynamic modulus was measured

Table 1
Melting point, crystallinity, Young's modulus and tensile strength of simultaneous biaxially stretched film. Annealing was done at 120°C for 20 min

Draw ratio (λ)	Melting point (°C)	Crystallinity (%)	Young's modulus (GPa)	Tensile strength (GPa)
1×1	226	2.50	1.65	0.011
1×1 (annealed)	226	8.68	1.86	0.021
2×2	226	4.73	2.78	0.045
2×2 (annealed)	226	32.61	2.89	0.062
3×3	226	6.39	4.25	0.123
3×3 (annealed)	227	36.09	4.29	0.151

by imposing a small dynamic strain to ensure the linear visco-elastic behavior of the specimen [26].

Table 1 summarizes the change of melting point, crystallinity, Young's modulus, and tensile strength for three kinds of specimens at $\lambda = 1\times1$, 2×2 and 3×3. The measurements were carried out using the specimens prepared by gelation/crystallization at 25°C. The melting point measured by differential scanning calorimetry (DSC) at 10°C min^{-1} is 226–227°C, which is independent of elongation. The crystallinity increases with increasing draw ratio and with annealing. In spite of the increase in crystallinity, the corresponding melting point is hardly affected. Young's modulus and tensile strength increase with the draw ratio. By preliminary experiments, the value at each draw ratio is found to be independent of the quenching temperature. Here it is of interest to consider the fact that Young's modulus of 4.3 GPa and tensile strength of 0.15 GPa at $\lambda = 3\times3$ are nearly equal to the respective maximum values, 4.4 GPa and 0.19 GPa, of a polyethylene film with $\lambda = 8.7\times8.7$.

Small angle light scattering (SALS) under Hv polarization condition was observed with a 15-mV He–Ne gas laser as a light source. The scattered intensity was too weak to be detected by photographic film, since most of beams could not pass through the analyzer. Therefore, the reflected pattern on the gel surface was detected using a commercial camera.

X-ray measurement was carried out with a 12-kW rotating-anode X-ray generator (Rigaku RDA-rA) operated at 200 mA and 40 kV. Here we must emphasize that the information concerning crystal orientation around the film normal direction cannot be obtained by using the usual X-ray diffraction for the present specimens because of very thin films (<5 μm). We developed a refined small instrument to stack a number of thin films as discussed in a previous paper [20]. In such a stacked condition, the measurement of the X-ray diffraction intensity distribution could be performed exactly using a horizontal scanning type goniometer, operating at a fixed time step scan of 0.1/40 s over a range of twice the Bragg angle $2\theta_B$ from 4 to 50° by rotating about the stretching direction at 2.5° intervals from 0 to 90°. The intensity distribution was measured as a function of a given rotational angle θ_j, corresponding to the polar angle between the reference axis and the reciprocal lattice vector of the j-th crystal plane. Corrections of X-ray diffraction intensity were made for air scattering, absorption, and amorphous contribution. The intensity curve thus obtained was assumed to be due to the contribution of the intensity from the crystalline phase. The intensity curve $I_{cry}(2\theta_B)$ was separated into the contributions from the individual crystal planes, assuming that each peak had a symmetric form given by a Lorenzian function as in Eq. (1), where I_j^0 is the maximum intensity of the j-th peak

$$I_{cry}(2\theta_B) = \sum_j \frac{I_j^0}{1 + (2\theta_0^j - 2\theta_B)^2/\beta_j^2}. \quad (1)$$

Here θ_j is the half-width of the j-th peak at half the peak intensity and θ_0^j the Bragg angle at which the maximum intensity of the j-th peak appears. Using the same process at a given θ_j in the range from 0 to 90°, the intensity distribution $I_j(\theta_j)$ can be determined for the respective j-th plane after integrating $I_{cry}(2\theta_B)$ by $2\theta_B$ at each θ_j, and consequently the orientation distribution function $2\pi q_j(\cos\theta_j)$ of the j-th reciprocal lattice vector may be given by

$$2\pi q_j(\cos\theta_j) = \frac{I_j(\theta_j)}{\int_0^{\pi/2} I_j(\theta_j)\sin(\theta_j)\,d\theta_j}. \quad (2)$$

Here it should be noted that there are some crystal planes whose Bragg angle reflections are located very close to each other. In this case, the function $2\pi q_j(\cos\theta_j)$ for the respective crystal planes cannot be represented because of the difficulty of peak separation. The composed function includes the contribution of several planes as follows:

$$2\pi q_j(\cos\theta_j) = 2\pi \sum_{i=1}^{N_j} C_{ji} q_{ji}(\cos\theta_{ji}). \quad (3)$$

The concept underlining Eq. (3) was first presented by Roe and Krigbaum [21–23]. N_i is the number of the j-th superposed peaks and C_{ji} the relative (normalized) weight for the vector $\mathbf{r}_{ji}$. Before numerical calculation by computer, initial values of C_{ji} are given by [27]

$$C_{ji} = \frac{F_{ji}^2}{\sum_{i=1}^{N_j} F_{ji}^2} \quad (4)$$

where F_{ji} is the structure factor of the j-th crystal plane. The orientation distribution function of crystallites can be calculated on the basis of the orientation functions of the

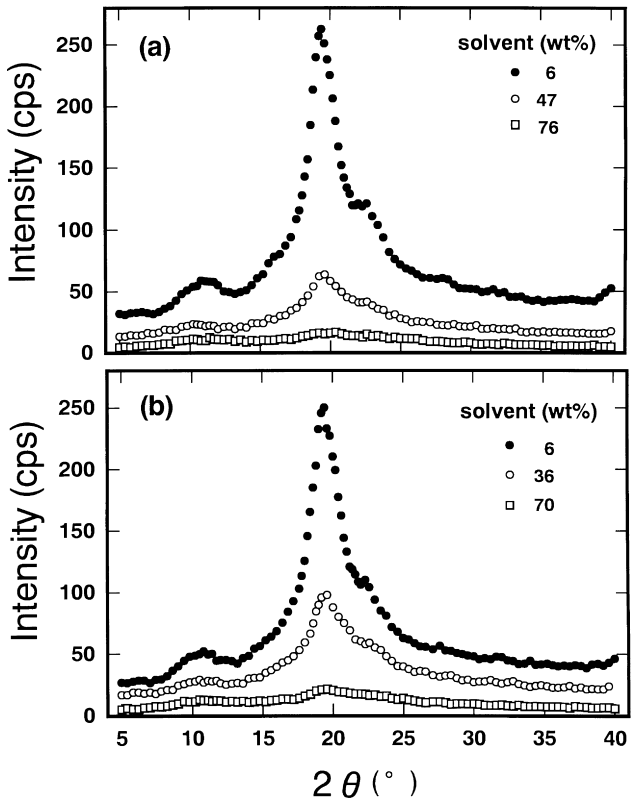

Fig. 1. WAXD intensity distribution of PVA gels with the indicated solvent contents. Gels were prepared by quenching the solution at: (a) 25°C and (b) −30°C.

reciprocal lattice vectors measured by X-ray diffraction, according to the method proposed by Roe and Krigbaum [21–23].

The ^{13}C CP/MAS (cross-polarization) and PST/MAS (pulse saturation transfer) NMR measurements were carried out for the dry gel films at 36 and 100°C with a JEOL, JM-EX270 spectrometer, operating at a static magnetic field of 6.34 T. A radio frequency of 67.8 MHz was used for detection of the ^{13}C resonance. The magic-angle spinning rate was 5–5.5 kHz. The contact time in the ^{13}C CP/MAS measurement was 2 ms. The chemical shifts were mainly determined from the higher field signal (29.5 ppm) of adamantane relative to tetramethylsilane (TMS). As special cases, the ^{13}C chemical shifts were determined by using the CH_2 line at 32.9 ppm of the orthorhombic crystalline component of polyethylene as an internal or external reference.

3. Results and discussion

3.1. Rubber elasticity of PVA gels

Fig. 1 shows the X-ray diffraction intensity curve as a function of solvent within the gels. The solvent content in the range of 80–90% was controlled by the adjustment of the concentration of the solution. The gel prepared by quenching the solution was stored for 1 h at room temperature without evaporating the solvent. For gels with solvent content <77%, the solvent content was determined by the weight change during the drying process from gel to film. This procedure was an indispensable method to prepare the gels, since uniform PVA solutions with high concentration could not be prepared because of their extremely high viscosity. To know the weight of the dry gel film, the gels were vacuum-dried for 2 days at 80–90°. In Fig. 1, the intensity curves are given after corrections for air-scattering, polarization and absorption. During the measurements, the evaporation of solvent was less than 3% and the content listed in this figure shows the values after the measurements. Parts (a) and (b) show the results for the gels that were prepared by quenching solutions at −30 and 25°, respectively. The X-ray diffraction curves for the two kinds of specimens show similar profiles at each solvent content indicating the similar crystallization behavior. The very weak broad peak associated with the overlapped reflection of the (110) and (1$\bar{1}$0) planes was observed around 19.5° for the gel with a 70% solvent content and the peak became sharper on decreasing the solvent content. For gels with the solvent content <47%, the reflection of the (200) appeared as a broad shoulder around 22° indicating an increase in crystallinity, and the peak became more distinct with further decrease in solvent content. Incidentally, the diffraction intensity from the gel with 80% solvent content provided a curve similar to a straight line indicating no reflection from ordered regions. With further increase in solvent content beyond 86%, the gels were too soft to carry out the X-ray measurement.

Fig. 2 shows SALS patterns under Hv polarization observed for the gels that were prepared by quenching solutions at 25°C. The photographs were taken after the gels had been stored for 1 h at room temperature without evaporating the solvent. The gel shows an X-type pattern in the very narrow range of solvent content indicating the existence of anisotropic rods, the optical axes being oriented parallel or perpendicular to the rod axis. Clear patterns could be observed for the gels with 87.7–87.4% solvent contents. In a previous work, it was confirmed that Hv scattering from the gel prepared from a 5% solution, the concentration of solution being 95%, also shows an X-type pattern when the gel was stored for more than 5 h. The pattern became more distinct with time as already reported [28]. Incidentally, no pattern could be observed for all the gels with a stored period of <20 min. On decreasing the solvent content to less than 87%, an X-type pattern becomes indistinct. Finally, the X-type lobes disappeared at a solvent content of <84%. A series of experimental results point out that the appearance of Hv pattern, indicating the existence of rod-like structures [29], is obviously independent of the progression of crystallization. If the formation of rods was due to the crystallization, the pattern must become distinct as the solvent content decreases. As one of the

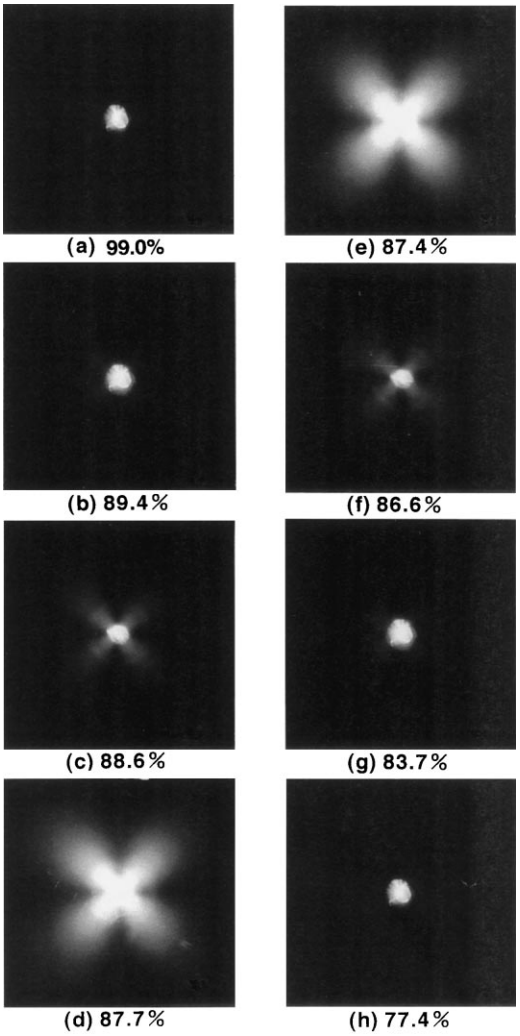

Fig. 2. Change of Hv SALS patterns of PVA gels with the indicated solvent contents which were prepared by quenching the solution at 25°C.

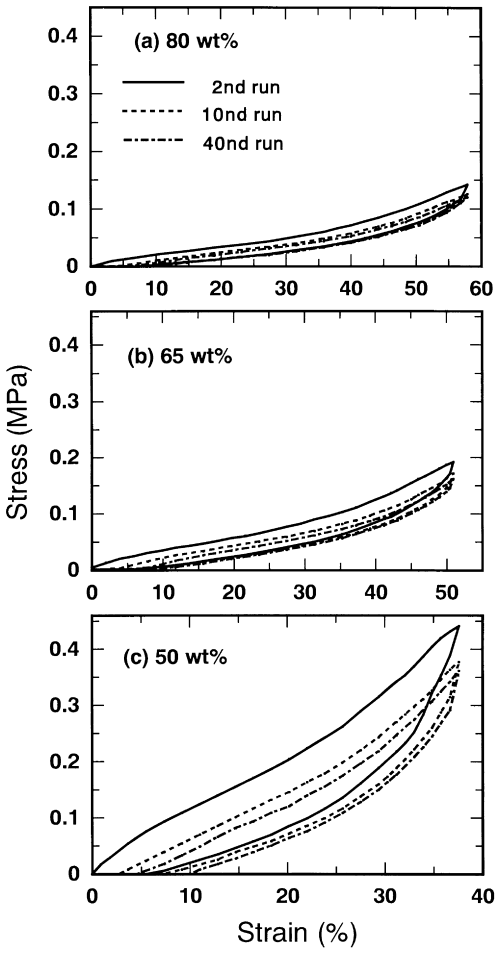

Fig. 3. Repeated curves of stress and strain for gels stretched up to 2 × 2 and recovered. Solvent contents are: (a) 80%; (b) 65% and (c) 50%.

possibilities, the formation of rods is thought to be due to the liquid–liquid phase separation by quenching solutions associated with spinodal decomposition [28–30]. Namely, PVA solutions at elevated temperature are thermodynamically unstable at the gelation temperature and tend to incur phase separation. In such supercooled solutions, compact molecular aggregates may be formed and then connect to the heterogeneous network system (polymer-rich phase). In spite of the ordering of molecules in the polymer-rich phase, the ordering does not allow the crystallization because of large amounts of solvent. No appearance of crystallites was confirmed by X-ray diffraction measurements. Accordingly, it may be concluded that the ordering structure in the polymer-rich phase forms optically anisotropic rods containing no crystallites. For the gels with solvent content $<84\%$, only an indistinct circular pattern was observed indicating the random array of quasi-crystallites smaller than the wavelength of the incident beam. The quasi-crystallites within gels with solvent content $<80\%$ cannot form its crystal lattice as detected by X-ray diffraction. The decrease in solvent content enhances the progression of crystallization as shown in Fig. 1 and the gels become stiffer. After evaporating the solvents, the resultant PVA film was transparent and showed no scattering under Hv polarization condition. This indicates that PVA crystallites did not form superstructures like spherulites or rods as have been observed for polyethylene [31] and polypropylene [32] dry gel films and the optical density fluctuation between small crystallites and the amorphous medium is very small. This concept supports the non-appearance of Hv pattern from any of the gels prepared by quenching the solution at -30°C. No change was observed during the process of solvent evaporation from a gel to form a film. Such rapid quenching prevents the concentration fluctuation to raise the phase separation because of the immobilization of the PVA chains at -30°C and causes immediately the appearance of a random array of quasi-crystallites much smaller than the wavelength of the incident beam without forming a super-structure as aggregation of quasi-crystallites like rods.

Fig. 3 shows repeated curves of stress–strain in the stretching direction when gels were stretched up to $\lambda = 2 \times 2$ and

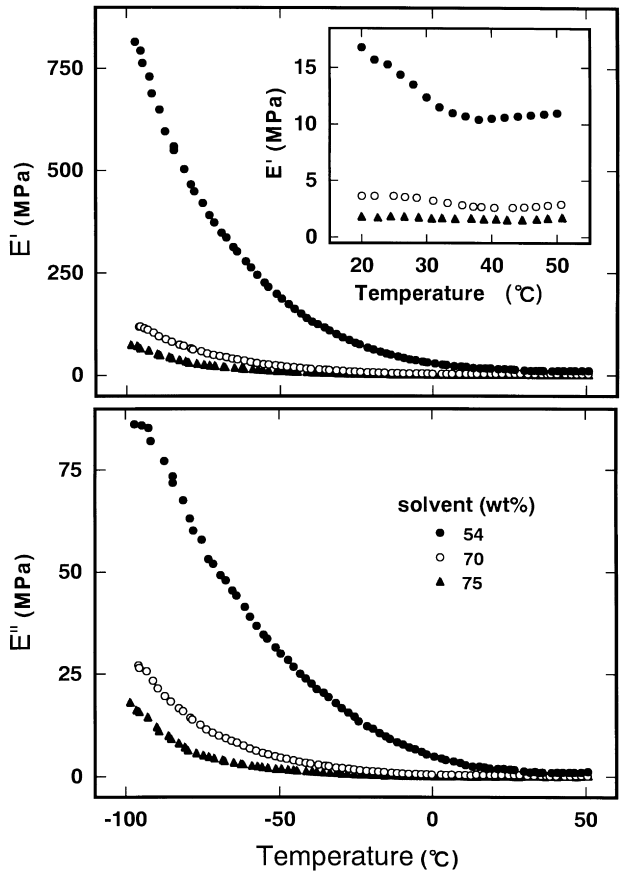

Fig. 4. Temperature dependence of storage and loss moduli for gels with the indicated solvent contents. Gels were prepared by quenching the solution at 25°C.

then recovered. Parts (a)–(c) show the behavior at the indicated solvent contents. The gels were prepared by quenching solutions at 25°C. The solvent content after the measurement was confirmed to be almost equal to that before the measurement. The difference is less than 2% within the experimental error. Interestingly, the repeated curves for the gel with 80% solvent content pass through almost the same route up to the 40th run. This behavior indicates the rubber elasticity because of negligible hysteresis under the stretching and recovering processes. Of course, X-ray measurements can detect very small crystallites with very large lattice disordering which play an important role as cross-linked points to cause the rubber elasticity. The gels with 87.7–87.4% solvent contents provide X-type patterns as shown in Fig. 2. They were too soft to obtain the stress–strain curve even at the 1st run. On decreasing the solvent content to 50%, the stress increases and the curve deviates from the recycle route indicating a large deviation from rubber elasticity.

A similar measurement was done for the gel with a 70% solvent content, prepared by quenching solutions at 25 and −30°C. The gels were stretched up to 1.2×1.2, 1.5×1.5 and 2×2 although the results are not shown in this paper. For the gel with $\lambda = 1.2 \times 1.2$, the repeated curves passed through about the same route. The curves deviated from the recycle route considerably with increasing draw ratio. The deviation became considerable for the gel with $\lambda = 2 \times 2$ with increasing repeated times.

Here it should be noted that such rubber elasticity was not confirmed for PVA gels prepared from aqueous solutions. The gels were too soft to be stretched. Even so, the X-ray diffraction intensity curve of the gels was similar to that for the gels prepared from Me_2SO and H_2O mixtures at the corresponding solvent content. No scattering could be observed under Hv polarization condition.

Fig. 4 shows the temperature dependence of the storage and loss moduli of the gels with the indicated solvent contents. The gels were prepared by quenching solutions at 25°C. The mixed solvent was confirmed not to be frozen at −130°C. In the preliminary experiment, the evaporation of solvent during heating process up to 30 and 50°C at a speed of 2°C min^{-1} were confirmed to be less than 3 and 5%, respectively, during the measurements. The storage and loss moduli show monotonous decreasing curves with increasing temperature. In the enlargement, it is seen that the very slight increase in the storage modulus with temperature could be observed in the range of 35–50°C characterizing rubber elasticity. This result supports the stress–strain behavior in Fig. 3. The increase in the storage modulus with decreasing temperature was observed at temperatures <0°C and the corresponding loss modulus also showed the same behavior with no peak associated with the amorphous dispersion and/or the local dispersion concerning motion of the side groups. In the temperature range of −50 to 10°C, the increase in the storage modulus with decreasing temperature is negligible for the gels with 75% solvent contents in comparison with the behavior of solid state discussed later. In contrast, the increase for the gels with 54% solvent content is due to drastic immobilization of molecular chains, which is probably attributed to the drastic increase in the number of cross-linking points because of an increase in crystallinity. The same phenomenon was also confirmed for gels prepared by quenching solutions at −30°C.

To facilitate understanding of the above behavior, temperature dependence of the storage and loss moduli of dry gel film is shown in Fig. 5. For undrawn (original) films, the storage modulus decreases drastically in the range of −80 to 30°C. The corresponding loss modulus shows two peaks at −10 and −70°C, respectively. Judging from the mechanical relaxation of polyethylene [33,34], the two peaks at −10 and −70°C are thought to be due to the amorphous dispersion and the local dispersion concerning the motion of the side groups, respectively. Accordingly, the large amorphous dispersion peak at −10°C is thought to be due to the friction at the grain boundary regions between the crystal and amorphous phases. Incidentally, the dry gel film prepared by aqueous solutions shows a similar behavior indicating a similar morphology in the solid state.

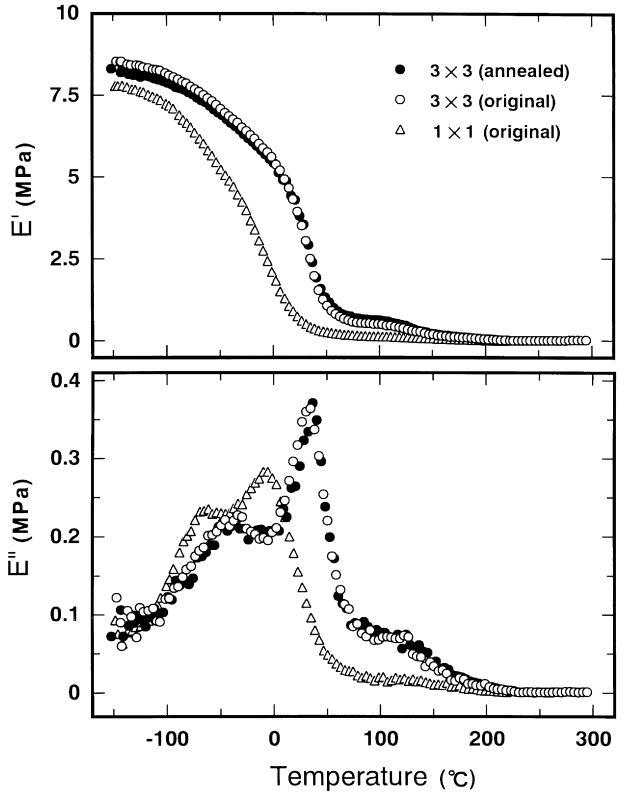

Fig. 5. Temperature dependence of storage and loss moduli for undrawn and drawn dry gel films. Gels were prepared by quenching the solution at 25°C.

3.2. Morphology and mechanical properties of dry gel films stretched biaxially

The swollen gels stretched up to $\lambda = 2 \times 2$ or $\lambda = 3 \times 3$ were kept in the stretcher and dried by dry airflow at room temperature. After drying, the specimens were removed from the stretcher. In another case, the specimens kept in the stretcher were annealed at 120°C for 30 min to promote an increase in crystallinity. The annealing temperature was chosen to avoid oxidation. When the specimen was removed from the stretcher, no dimensional change was observed. As listed in Table 1, the crystallinity increased drastically but the corresponding Young's modulus is hardly affected by the annealing. Young's modulus at 20°C is almost equal to that of polyethylene with $\lambda = 8.7 \times 8.7$. This means that the biaxially stretched PVA has an advantage as commercial films with better mechanical property in spite of low draw ratio.

To pursue the detailed relationship between mechanical property and molecular orientation by a linear elastic theory, the orientation of crystallites must be estimated in terms of the orientation distribution function of crystallites calculated from the orientation distribution function of the reciprocal vectors of the crystal planes. The orientation function of crystallites is important to calculate Young's modulus based on a linear elastic theory. For this purpose, we set following geometrical arrangements.

Fig. 6a shows Cartesian coordinate 0-$U_1U_2U_3$ fixed within a structural unit, with respect to another Cartesian coordinate 0-$X_1X_2X_3$ fixed in a bulk specimen. The U_3-axis may be taken along the c-axis. In the system of simultaneous biaxially stretched films, crystallites have a random orientation around the X_3-axis (the film thickness direction). The orientation of the structural unit within the space of the film specimen may be specified by using three Euler angles, θ, ϕ and η. The angles θ and ϕ, which define the orientation of the U_3-axis of the unit within the space, are polar and azimuthal angles, respectively, and η specifies the rotation of the unit around its own U_3-axis. Coordinates (b) and (c) show a given j-th axis $\mathbf{r}_j$ within the unit, specified by the polar angle θ_j and the azimuthal angle ϕ_j with respect to the Cartesian coordinate 0-$X_1X_2X_3$ and specified by polar angle Θ_j and the azimuthal angle Φ_j with respect to the 0-$U_1U_2U_3$ of the unit, respectively. Table 2 shows the values of Θ_j and Φ_j Furthermore, the values of the three principle crystallographic axes, the a-, b-, and c-axes in the present system are listed together.

For an uniaxial system around the X_3-axis, the orientation

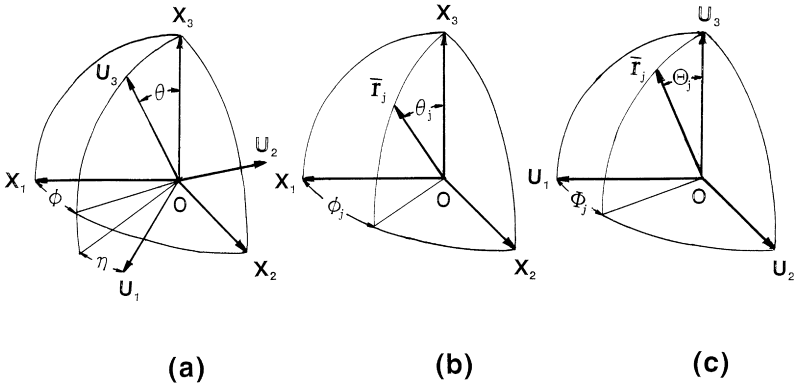

Fig. 6. Cartesian coordinate illustrating the geometrical relation: (a) Euler angles θ and η which specify the orientation of coordinate 0-$U_1U_2U_3$ of structural unit with respect to coordinate 0-$X_1X_2X_3$ of specimen; (b) angles θ_j and ϕ_j which specify the orientation of the given j-th axis of the structural unit with respect to the coordinate 0-$X_1X_2X_3$; (c) angles Θ_j and Φ_j which specify the orientation of the j-th axis of the structural unit with respect to the coordinate 0-$U_1U_2U_3$.

Table 2
Diffraction angle $2\theta_B$, and polar and azimuthal angles Θ_j and Φ_j with regard to the orientation of the reciprocal lattice vector of the j-th crystal plane within the poly(vinyl alcohol) crystal unit

(*hkl*)	$2\theta_B$	Θ_j	Φ_j
(110)	20.10	90.0	53.00
(1$\bar{1}$0)	19.24	90.0	56.55
(210)	28.57	90.0	34.40
(2$\bar{1}$0)	27.32	90.0	143.83
(200)	22.74	90.0	0.00
(010)	16.04	90.0	87.34
(3$\bar{1}$0)	37.45	90.0	152.26
(220)	40.86	90.0	53.00
(2$\bar{2}$0)	39.04	90.0	56.55
a-Axis		90.0	−2.50
b-Axis		90.0	90.00
c-Axis		0.00	0.00

distribution function $\omega(\theta,\phi)$ of crystallites may be calculated from the orientation distribution function of the reciprocal lattice vector of the j-th plane, $2\pi q_j(\cos\theta_j)$, by using a method proposed by Roe and Krigbaum [21–23]

$$F^j_{\ell 0} = \langle P_\ell(\cos\theta_j)\rangle = \int_0^{2\pi}\int_0^{\pi} q_j(\cos\theta_j)P_\ell(\cos\theta_j)\sin\theta_j\,\mathrm{d}\theta_j\,\mathrm{d}\phi_j, \tag{5}$$

$$F^j_{\ell 0} = F_{\ell 00}\sum_{i=1}^{N_i} C_{ji}P_\ell(\cos\Theta_{ji}) + 2\sum_{n=2}^{\ell}\frac{(\ell-n)!}{(\ell+n)!}\left\{F_{\ell 0n}\sum_{i=1}^{N_i} C_{ji}P^n_\ell(\cos\Theta_{ji})\cos n\Phi_{ji} + G_{\ell 0n}\sum_{i=1}^{N_i} C_{ji}P^n_\ell(\cos\Theta_{ji})\sin n\Phi_{ji}\right\}, \tag{6}$$

$$4\pi^2\omega(\theta,\eta) = \frac{1}{2} + \sum_{\ell=2}^{\infty}\left[\frac{(2\ell+1)}{2}\left\{F_{\ell 00}P_\ell(\cos\theta) + 2\sum_{n=2}^{\ell}\frac{(\ell-n)!}{(\ell+n)!}(F_{\ell 0n}\cos n\eta + G_{\ell 0n}\sin n\eta)P^n_\ell(\cos\theta)\right\}\right]. \tag{7}$$

Here ℓ and n are even integers. $P^n_\ell(X)$ and $P_\ell(X)$ are the associated Legendre polynomials and Legendre polynomials, respectively. $F^j_{\ell 0n}$, $F_{\ell 0n}$ and $G_{\ell 0n}$ are the coefficients. $F^j_{\ell 0n}$ is the ℓ-th order orientation factor of the j-th crystal plane estimated by X-ray diffraction, and therefore the generalized orientation factors $F_{\ell 0n}$ and $G_{\ell 0n}$, can be determined by solving the linear equations represented by Eq. (6), since there exist more equations than the number of unknowns, as was pointed out by Roe and Krigbaum [21–23].

In accordance with Roe and Krigbaum, the values of $F_{\ell 0n}$ and $G_{\ell 0n}$ were determined by the least-squares method. The value of C_{ji}, where the initial value is given by Eq. (4), were determined by the simplex method [35], which is a direct research method to obtain the object function on the basis of trial and error. To compare the observed $2\pi q_j(\cos\theta_j)$ with those calculated for the respective crystal planes, we recalculated $F^j_{\ell 0}$ in turn from $F_{\ell 0n}$ and $G_{\ell 0n}$, which were initially determined by the weighted least-squares method by the use of Eq. (6), and further calculated the observed $2\pi q_j(\cos\theta_j)$ from the recalculated $F^j_{\ell 0}$ by the use of Eq. (8):

$$2\pi q_j(\cos\theta_j) = \frac{1}{2} + \sum_{\ell=2}^{\infty}\frac{2\ell+1}{2}F^j_{\ell 0}P_\ell(\cos\theta_j). \tag{8}$$

The calculation was continued until the best fit was achieved within the capability of the simplex method [35]. Using the final values of the parameters, a mean-square error R between the calculated $F^j_{\ell 0}$ and the recalculated $F^j_{\ell 0}$ may be defined as follows:

$$R = \frac{\sum_j\sum_\ell \rho_j\{(F^j_{\ell 0})_{\mathrm{cal}} - (F^j_{\ell 0})_{\mathrm{recal}}\}^2}{\sum_j\sum_\ell \rho_j\{(F^j_{\ell 0})_{\mathrm{cal}}\}^2} \tag{9}$$

where ρ_j is weighting factors required in the least-squares calculation. As a first approximation, the initial values of ρ_j were assumed to be proportional to a square of the structure factor and were subsequently modified to obtain the best fit between experimental and calculated results through numerical calculations by a computer [27]. The introduction of ρ_j is due to the fact that $2\pi q_j(\cos\theta_j)$ of the crystal plane with high diffraction intensity provide high accuracy but $2\pi q_j(\cos\theta_j)$ of less accurately measured crystal planes contain large experimental error. Namely, the value of ρ_j to determine $F_{\ell 0n}$ and $G_{\ell 0n}$ becomes larger for crystal planes with higher diffraction intensity.

Figs. 7 and 8 compare the observed $2\pi q_j(\cos\theta_j)$ with those recalculated for the respective crystal planes for the films with $\lambda = 2\times 2$ and 3×3, respectively. Fig. 9a and b shows the superposed functions of $2\pi q_j(\cos\theta_j)$ of the crystal planes (3$\bar{1}$0), (220), and (2$\bar{2}$0) at $\lambda = 2\times 2$ and 3×3, respectively. The function of the (220) and (2$\bar{2}$0) crystal planes must be essentially equal to those of (110) and (1$\bar{1}$0). However, as discussed before, the peak separation of these crystal planes were impossible and the separated function of (3$\bar{1}$0) could not be observed directly. Incidentally, the orientation function of the (3$\bar{1}$0) plane is indispensable to obtain $\omega(\theta,\eta)$ calculated using Eq. (7) with the coefficients $F_{\ell 0n}$ and $G_{\ell 0n}$ determined from Eq. (6) with ℓ limited to 6. We calculated $F^j_{\ell 0}$ from Eq. (6) to minimize the value of R in Eq. (9). After that, we recalculated $F^j_{\ell 0}$, in turn, from the values of $F_{\ell 0n}$ and $G_{\ell 0n}$, and further calculated $2\pi q_j(\cos\theta_j)$ from the recalculated $F^j_{\ell 0}$ value using Eq. (8). The values of R in Eq. (8) was 9.1% at $\lambda = 2\times 2$, and 9.7% at $\lambda = 3\times 3$, respectively.

Returning to Figs. 7 and 8, it is evident that fairly good

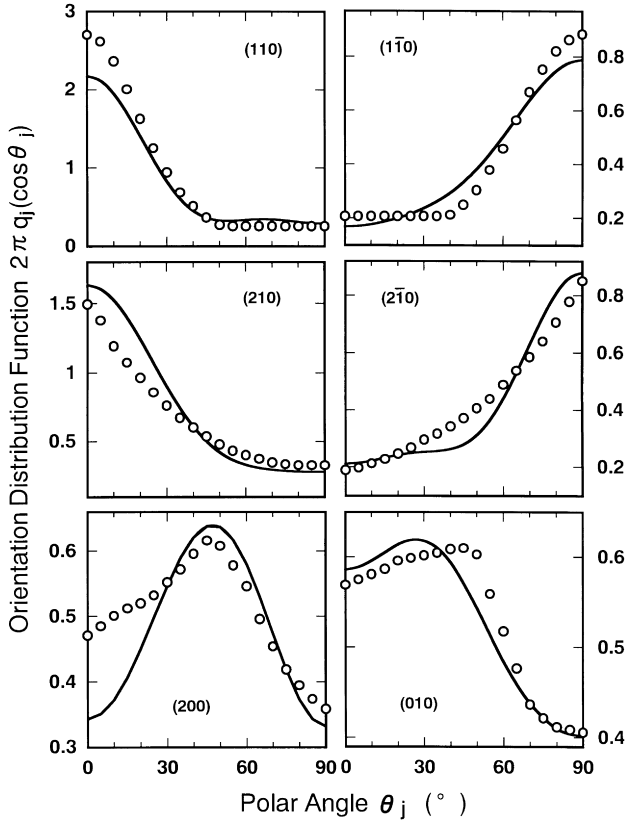

Fig. 7. Orientation distribution functions $2\pi q_j(\cos\theta_j)$ of the reciprocal lattice vectors of the indicated crystal planes of a PVA film with a draw ratio of 2×2. Circles: values obtained from experiment. Solid curves: values calculated with the 6-term series.

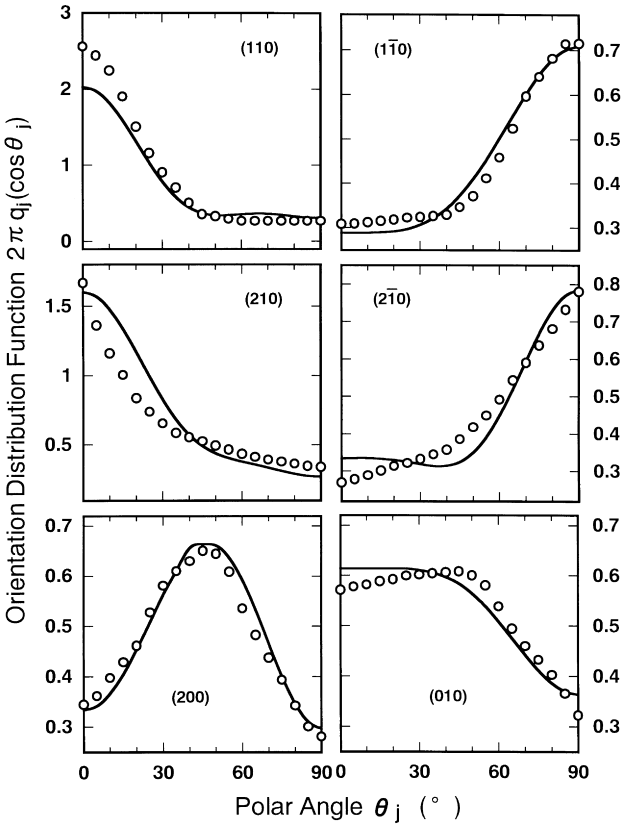

Fig. 8. Orientation distribution functions $2\pi q_j(\cos\theta_j)$ of the reciprocal lattice vectors of the indicated crystal planes of a PVA film with a draw ratio of 3×3. Circles: values obtained from experiment. Solid curves: values calculated with the 6-term series.

agreement between the observed and calculated distribution functions of the reciprocal lattice vectors of the indicated crystal planes was obtained, even for less accurately measured crystal planes with lower weighting factors. In Fig. 7, $2\pi q_j(\cos\theta_j)$ concerning the (110) and (1$\bar{1}$0) planes have a sharp peak at 0 and 90°, respectively, while $2\pi q_j(\cos\theta_j)$ concerning the (200) and (010) planes have a sharp peak and a broad peak at 45°, respectively. Judging from the preferential orientation of the (110) plane parallel to the film surface, it may be expected that the *c*-axes are also oriented parallel to the film surface. Such a characteristic mode with the preferential orientation of the specific plane has been observed for several crystalline polymers such as polyethylene [20] and polypropylene [11]. The behavior observed for a series of crystalline polymers is thought to be due to the slippage of the specific crystal plane with the highest atomic density within the crystal unit in the stretching direction due to the generated planar stress during biaxially stretching. The functions $2\pi q_j(\cos\theta_j)$ of the *j*-th crystal plane in Fig. 8 shows a similar profile to those in Fig. 7. But each function in Fig. 8 becomes slightly sharper indicating the further increase in orientational degree of crystallites with increasing draw ratio. However, it is very difficult to postulate the orientational behavior of the principle crystallographic axes, *a*-, *b*-, and *c*-axes, from the observed orientation function of the *j*-th crystal plane. To obtain this information, $F^j_{\ell 0}$ for the *a*-, *b*-, and *c*-axes must be calculated from the orientation distribution function of crystallites $\omega(\theta,\eta)$. Accordingly, the orientation distribution functions of crystallites are proposed to give the quantitative analysis of the complicated orientational behavior.

Fig. 10a and b shows the orientation distribution functions of crystallites, $\omega(\theta,\eta)$, for the PVA films with $\lambda = 2\times2$

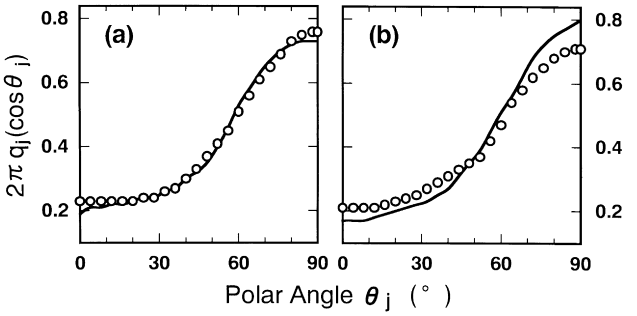

Fig. 9. Orientation distribution functions $2\pi q_j(\cos\theta_j)$ of the reciprocal lattice vector of the superposed crystal planes (3$\bar{1}$0), (220) and (2$\bar{2}$0) of PVA film with draw ratios: (a) 2×2 and (b) 3×3. Circles: values obtained from experiment. Solid curve: values calculated with the 6-term series.

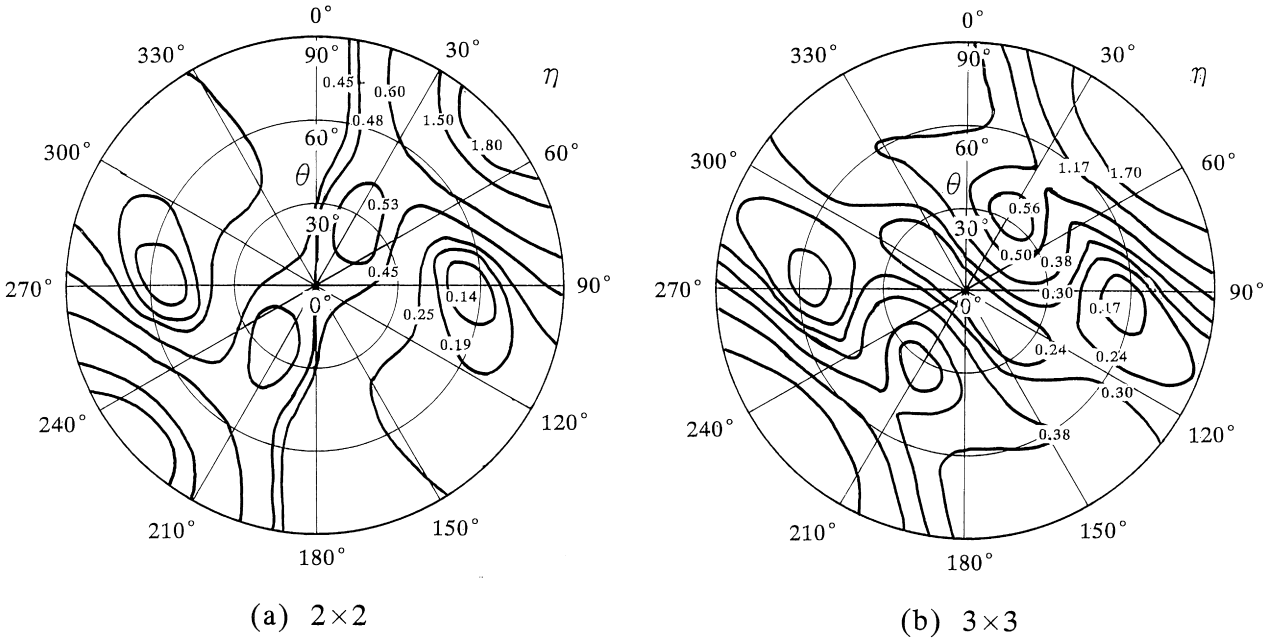

Fig. 10. Orientation distribution functions of crystallites $4\pi^2\omega(\theta, \eta)$ calculated by Eqs. (5)–(7): (a) a drawn film with 2×2 and (b) a drawn film with 3×3.

and 3×3, respectively. Because of a monoclinic form of the PVA crystal unit, the map is symmetric at η and $\pi + \eta$ and is more complicated in comparison with an orthorhombic form like the polyethylene crystal unit [20]. The two maps a and b are essentially similar showing two highly populated regions and a lowly populated region. The detailed observation reveals that the counters in map b are slightly steeper than those in map a indicating the further orientation of crystallites with increasing draw ratio. The two maps reveal that the density is the highest at $\theta = 90°$ and $\theta = 45°$ indicating the preferential orientation of the *c*-axes parallel to the film surface and the considerable η-dependence due to the specific rotation of crystallites around the *c*-axes. This is obviously attributed to the preferential orientation of the (110) plane parallel to the film surface. In map a, there is a peak at $\theta = 28°$ and $\eta = 32°$ and a valley $\theta = 55°$ and $\eta = 95°$, respectively, and in map b, a peak at $\theta = 32°$ and $\eta = 30°$ and a valley at $\theta = 55°$ and $\eta = 100°$, respectively. The existence of the peaks and valleys cannot be recognized definitely from the orientation function of the *j*-th crystal plane but the appearance suggests two possibilities. One is the real peak and the valley associated with the orientation of crystallites, while the other, the artifact due to the expansion of the sharp experimental function of $2\pi q_j(\cos\theta_j)$ into infinite series of spherical harmonics. This shall be discussed later.

The orientation distribution functions of the *a*-, *b*-, and *c*-axes can be determined by substituting the values of Θ_j and Φ_j for each axis in Table 2 into Eq. (6) and by using Eq. (8). Fig. 11 shows the results at the indicated draw ratios. Interestingly, the orientation function of the *c*-axis at $\lambda = 2 \times 2$ does not show a monotonous increasing curve and has two peaks at $\theta_j = 0$ and 90°, respectively. Certainly, the peak at $\theta_j = 90°$ indicates the preferential orientation of the *c*-axis parallel to the film surface, while the duller peak at $\theta_j = 0°$ appears automatically to make the valley around $\theta_j = 50°$ corresponding to $\theta = 55°$ in Fig. 10a. Such behavior still remains an unresolved problem. The orientation of the *a*-axis

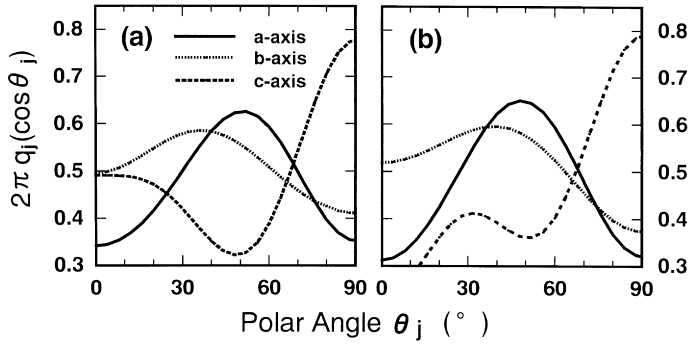

Fig. 11. Orientation distribution functions $2\pi q_j(\cos\theta_j)$ of the *a*-, *b*- and *c*-axes: (a) a drawn film with 2×2 and (b) a drawn film with 3×3.

has a sharp peak around 50°, while that of the *b*-axis shows a duller peak around 40°. These orientational modes are affected by the preferential orientation of the (110) plane. The orientation function of the *c*-axis at $\lambda = 3 \times 3$ has two peaks at $\theta_j = 90$ and 32°, respectively. The higher peak at $\theta_j = 90°$ is due to the preferential orientation of the *c*-axes parallel to the film surface but the other peak at $\theta_j = 32°$ cannot be explained. Even so, the latter peak is not the artifact due to the expansion of the sharp experimental function of $2\pi q_j(\cos\theta_j)$ into infinite series of spherical harmonics. This is surely attributed to the somewhat complicated orientation behavior of the *c*-axes reflecting to the orientation behavior of crystallites showing the peak at $\theta = 32°$ and $\eta = 30°$, and the valley at $\theta = 55°$ and $\eta = 100°$ in Fig. 10b. Anyway, the orientations of the *a*-, *b*-, and *c*-axes give one of the important clues to know the detailed information of the orientation behavior of the crystallites, and this information cannot be absolutely derived from the simple evaluation as the level of the second-order orientation factors of several crystal planes has been generally done.

In order to estimate the orientation behavior of crystallites within the dry gel films, the second-order orientation factor of the amorphous chain segments was obtained from the birefringence as estimated by the subtraction of the crystalline contribution from the total birefringence, assuming simple additivity as indicated in the following equation [36]:

$$\Delta_{\text{total}} = X_c\Delta_c + (1 - X_c)\Delta_a + \Delta_f \tag{10}$$

where Δ_{total} is the total birefringence of the bulk specimen, Δ_c the crystalline birefringence, Δ_a the non-crystalline birefringence, X_c the volume fraction of the crystalline phase, and Δ_f the form birefringence. Δ_c and Δ_a are given by

$$\begin{aligned}\Delta_c &= n_a F_{200}^{[200]} + n_b F_{200}^{[020]} + n_c F_{200}^{[002]} \\ &= (n_c - n_a)F_{200}^{[002]} + (n_b - n_a)F_{200}^{[020]}\end{aligned} \tag{11}$$

and

$$\Delta_a = (n_\parallel - n_\perp)F_{200}^{\text{am}} \tag{12}$$

where n_a, n_b, and n_c are the refractive indices along the *a*, *b*, and *c*-axes, which are given as 1.737, 1.717, and 1.827, respectively. $n_\parallel$ and $n_\perp$ are the refractive indices parallel and perpendicular to an amorphous chain segment. The intrinsic birefringence of $(n_\parallel - n_\perp)$ of the amorphous chain segment is 88×10^{-3} and F_{200}^{am} is the second-order orientation factor of the amorphous chain segments. The procedure for evaluating the intrinsic birefringence of crystalline and amorphous phases is quite similar to that described earlier [37]. These values were estimated by utilizing the values of bond polarizabilities proposed by Clement [38], the crystal structure by Nitta et al. [39] and the value of intrinsic crystalline and amorphous densities (1.345 and 1.269, respectively) by Sakurada et al. [25]. The orientation factors, F_{200} and F_{200}^{am}, characterize the molecular orientation distribution with variation between $-1/2$ and 1. In a simultaneous biaxially stretched film, they are 0 for random orientation, while for complete orientation parallel and perpendicular to the film normal direction, they are unity and $-1/2$, respectively.

By neglecting Δ_f, the orientation factors of the *c*-axes and the amorphous chain segments may be obtained through Eqs. (10)–(12). For the film with $\lambda = 2 \times 2$, F_{200} for crystallites and F_{200}^{am} for amorphous chain segments are -0.0779 and -0.0876, respectively, while for the film with 3×3, F_{200} and F_{200}^{am} are -0.146 and -0.154, respectively. The preferential orientational degree of the amorphous chain segments is higher than that of the *c*-axes. This indicates that the preferential orientation of the *c*-axes in the stretching direction is due to straining tie molecules and the planar orientation of the (110) plane is attributed to the rotation of crystallites around its own *c*-axis which is caused by the slippage of crystallites on the (110) plane. Unfortunately, it was very difficult to judge whether this process accompanies the crystal transformation from a folded to a fibrous type, since small angle X-ray scattering and density results provided no significant information.

The slippage of the crystallites on the (110) plane is probably thought to be due to out of the framework of rubber elasticity of swollen gels shown in Fig. 3. Unfortunately, it was impossible to check the preferential orientation of the (110) plane of the swollen gels assuring rubber elasticity by X-ray diffraction because of very weak reflection of the superposed peak of the (110) and $(1\bar{1}0)$ planes. The original (not annealed) dry gel film with $\lambda = 2 \times 2$ showing crystal plasticity, however, gave the same orientation function of crystallites showing the same preferential orientation as those of the corresponding annealed film. Accordingly, the slippage was less significant within the swollen gels assuring rubber elasticity and the evaporation of the solvent promoted the slippage within the fixed specimen. Actually, the repeated curve for the gels with 50% solvent content deviated from the recycle route drastically indicating the slippage associated with crystal plasticity.

3.3. Young's modulus of simultaneous biaxial films estimated from crystal and amorphous orientation functions

Young's modulus of a biaxially stretched film can be calculated by using the generalized orientation factors $F_{\ell 0n}$ and $G_{\ell 0n}$ on the basis of a two-phase model assuming the homogeneous stress hypothesis for a polycrystalline material [40]. This treatment on a linear elastic theory is somewhat complicated but realistic. The treatment represented as a continuous body is especially suitable for the present biaxially stretched film. In the present specimens, no scattering pattern from aggregation of crystallites such as spherulites and rod-like textures was observed under Hv polarization condition.

Fig. 12 shows the model to satisfy the above concept

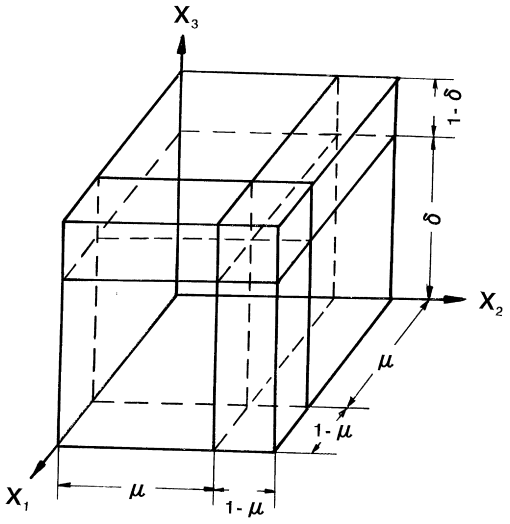

Fig. 12. A composite model in which oriented crystallites are surrounded by an anisotropic amorphous phase.

[41,42]. The proposed model includes polymeric systems with a low degree of molecular orientation and low crystallinity, in which the oriented crystalline layers are surrounded by an anisotropic amorphous phase. Assuming that crystal unit is set in this field, the crystal strains can be represented as a function of composite mode and molecular orientation. This means that the oriented crystallites are surrounded by an anisotropic amorphous phase where amorphous chain segments are oriented predominantly in the stretching direction. This model system satisfies the morphological characteristics of a specimen with low crystallinity like PVA specimens. Volume crystallinity X_c is represented by $\delta\mu^2$ by the use of the fraction lengths δ and μ in the directions of X_3 and X_2 (and X_1) axes. In this model system, the amorphous layers are adjacent to the oriented crystalline layers with the interfaces perpendicular to the X_1, X_2 and X_3 axes. Strains of the two phases at the boundary are assumed to be identical. This model can be constructed by following three processes. First, an anisotropic amorphous layer lies adjacent to the crystallite with the interface perpendicular to the X_3 axes and the resultant system is termed as phase I. Secondly, an anisotropic amorphous layer with fraction length $1-\mu$ is attached to the structure of phase I in a plane normal to the X_1 direction to construct phase II. The final phase III can be constructed by adding an anisotropic amorphous layer with fraction length $1-\mu$ to phase II. This procedure was represented elsewhere in detail [41]. For simultaneous biaxially stretched films, this model corresponds to a series model at $\mu = 1$, while it corresponds to a parallel model at $\delta = 1$. In following discussion, some final equations are described to shorten this paper. Complicated mathematical derivation was eliminated, since such treatment is similar to that of crystal lattice modulus reported elsewhere [41,42].

In accordance with the mathematical procedure of the generalized Hook's law, Young's modulus in the stretching direction (the X_1 and X_2 directions) can be given by

$$E = \frac{\mu}{S_{11}^{\mathrm{II}}} + \frac{1-\mu}{S_{11}^{\mathrm{av}}} + \frac{\left\{\dfrac{S_{13}^{\mathrm{II}}}{S_{11}^{\mathrm{II}}} - \dfrac{S_{13}^{\mathrm{av}}}{S_{11}^{\mathrm{av}}}\right\}^2}{\dfrac{S_{33}^{\mathrm{II}}}{\mu}\left\{1 - \dfrac{S_{13}^{\mathrm{II}^2}}{S_{11}^{\mathrm{II}} S_{33}^{\mathrm{II}}}\right\} + \dfrac{S_{33}^{\mathrm{av}}}{1-\mu}\left\{1 - \dfrac{S_{13}^{\mathrm{av}^2}}{S_{11}^{\mathrm{av}} S_{33}^{\mathrm{av}}}\right\}}. \quad (13)$$

In Eq. (13), S_{ij}^{II} is given as a function of S_{ij}^{I}, S_{ij}^{av} and μ, and S_{ij}^{I} is also given as a function of S_{ij}^{cv}, S_{ij}^{av} and δ in which S_{ij}^{cv} and S_{ij}^{av} are the average compliances of the crystal and amorphous phases, respectively. The complicated relationship was represented by Matsuo elsewhere [41].

The relation between the intrinsic compliance of the structural unit and the bulk compliance is given by

$$S_{ijk\ell}^{\mathrm{cv}} = \sum_{r=1}^{3}\sum_{q=1}^{3}\sum_{p=1}^{3}\sum_{o=1}^{3} \langle a_{io}a_{jp}a_{kq}a_{\ell r}\rangle_{\mathrm{cv}} S_{opqr}^{\mathrm{co}}, \quad (14)$$

$$S_{ijk\ell}^{\mathrm{av}} = \sum_{r=1}^{3}\sum_{q=1}^{3}\sum_{p=1}^{3}\sum_{o=1}^{3} \langle a_{io}a_{jp}a_{kq}a_{\ell r}\rangle_{\mathrm{av}} S_{opqr}^{\mathrm{ao}}, \quad (15)$$

$S_{ijk\ell}^{\mathrm{cv}}$ and $S_{ijk\ell}^{\mathrm{av}}$ are bulk compliances of the crystal and amorphous phases, respectively, and S_{opqr}^{co} and S_{opqr}^{ao} are their intrinsic compliances. a_{io} is, for example, the direction cosine of the U_o-axis with respect to the X_i-axis, which is given from the geometrical arrangements in the previous paper [20]. Average values of the crystal phase in Eq. (14), $\langle a_{io}a_{jp}a_{kq}a_{lr}\rangle_{\mathrm{cv}}$ are given by

$$\langle a_{io}a_{jp}a_{kq}a_{lr}\rangle_{\mathrm{cv}} = \int_0^{2\pi}\int_0^{2\pi}\int_0^{\pi} \omega(\theta,\eta) a_{io}a_{jp}a_{kq}a_{lr} \sin\theta \,\mathrm{d}\theta \,\mathrm{d}\phi \,\mathrm{d}\eta \quad (16)$$

where $\omega(\theta,\eta)$ is the orientation distribution function of the crystal unit 0-$U_1U_2U_3$ with respect to the coordinate 0-$X_1X_2X_3$ in Fig. 6. On the other hand, average values of the amorphous phase in Eq. (15), $\langle a_{io}a_{jp}a_{kq}a_{lr}\rangle_{\mathrm{av}}$ are given by

$$\langle a_{io}a_{jp}a_{kq}a_{lr}\rangle_{\mathrm{av}} = \int_0^{2\pi}\int_0^{2\pi}\int_0^{\pi} \omega_{\mathrm{am}}(\theta) a_{io}a_{jp}a_{kq}a_{lr} \sin\theta \,\mathrm{d}\theta \,\mathrm{d}\phi \,\mathrm{d}\eta \quad (17)$$

where $\omega_{\mathrm{am}}(\theta)$ is an orientation distribution function of the amorphous chain segments. The generalized orientation factors $F_{\ell 0n}$ and $G_{\ell 0n}$ of the crystal phase and F_{l00}^{am} of the amorphous phases can be represented by using $\omega(\theta,\eta)$ and $\omega_{\mathrm{am}}(\theta)$, respectively, in the case when both the structural units have an uniaxial orientation around the X_3-axis (film

thickness direction):

$$F_{\ell 0n} = \int_0^{2\pi}\int_0^{2\pi}\int_0^{\pi} \omega(\theta,\eta)P_\ell^n(\cos\theta)\cos n\eta \sin\theta \,\mathrm{d}\theta\,\mathrm{d}\phi\,\mathrm{d}\eta, \tag{18}$$

$$G_{\ell 0n} = \int_0^{2\pi}\int_0^{2\pi}\int_0^{\pi} \omega(\theta,\eta)P_\ell^n(\cos\theta)\sin n\eta \sin\theta \,\mathrm{d}\theta\,\mathrm{d}\phi\,\mathrm{d}\eta \tag{19}$$

and

$$F_{\ell 0n}^{\mathrm{am}} = \int_0^{2\pi}\int_0^{2\pi}\int_0^{\pi} \omega_{\mathrm{am}}(\theta)P_\ell(\cos\theta)\sin\theta \,\mathrm{d}\theta\,\mathrm{d}\phi\,\mathrm{d}\eta. \tag{20}$$

For an orthorhombic crystal form like polyethylene, $G_{\ell 0n} = 0$. The elastic compliance $S_{ijk\ell}$ represented as a tensor quantity may be related to S_{uv} by the matrix as shown in the previous paper [43].

Using Eqs. (14)–(20), for example, S_{11}^{cv} $(= S_{22}^{\mathrm{cv}})$ of the crystal unit and S_{11}^{av} $(= S_{22}^{\mathrm{av}})$ of the amorphous unit in the stretching direction may be given as follows:

$$\begin{aligned}
S_{11}^{\mathrm{cv}} = S_{22}^{\mathrm{cv}} = {} & \frac{1}{64}S_{11}^{\mathrm{co}}\left\{\frac{1}{35}F_{404} - \frac{8}{35}F_{402} + \frac{72}{35}F_{400}\right. \\
& \left. - \frac{32}{7}F_{202} + \frac{64}{7}F_{200} + \frac{64}{5}\right\} + \frac{1}{64}S_{22}^{\mathrm{co}}\left\{\frac{1}{35}F_{404}\right. \\
& \left. + \frac{8}{35}F_{402} + \frac{72}{35}F_{400} + \frac{32}{7}F_{202} + \frac{64}{7}F_{200} + \frac{64}{5}\right\} \\
& + S_{33}^{\mathrm{co}}\left\{\frac{3}{35}F_{400} - \frac{2}{7}F_{200} + \frac{1}{5}\right\} - \frac{1}{64}(2S_{12}^{\mathrm{co}} + S_{66}^{\mathrm{co}}) \\
& \times\left\{\frac{1}{35}F_{404} - \frac{24}{35}F_{400} - \frac{64}{21}F_{200} - \frac{64}{15}\right\} \\
& + \frac{1}{8}(2S_{13}^{\mathrm{co}} + S_{55}^{\mathrm{co}})\left\{\frac{2}{35}F_{402} - \frac{12}{35}F_{400} - \frac{2}{21}F_{202}\right. \\
& \left. - \frac{4}{21}F_{200} + \frac{8}{15}\right\} - \frac{1}{8}(2S_{23}^{\mathrm{co}} + S_{44}^{\mathrm{co}})\left\{\frac{1}{35}F_{402}\right. \\
& \left. + \frac{12}{35}F_{400} - \frac{2}{21}F_{202} + \frac{4}{21}F_{200} - \frac{8}{15}\right\} \\
& - \frac{1}{32}S_{16}^{\mathrm{co}}\left\{\frac{1}{35}G_{404} - \frac{4}{35}G_{402} - \frac{16}{7}G_{202}\right\} \\
& + \frac{3}{112}S_{26}^{\mathrm{co}}\left\{\frac{1}{35}G_{404} + \frac{4}{35}G_{402} + \frac{16}{7}G_{202}\right\}
\end{aligned} \tag{21}$$

and

$$\begin{aligned}
S_{11}^{\mathrm{av}} = S_{22}^{\mathrm{av}} = {} & \frac{1}{8}(S_{11}^{\mathrm{ao}} + S_{22}^{\mathrm{ao}})\left\{\frac{9}{35}F_{400}^{\mathrm{am}} + \frac{8}{7}F_{200}^{\mathrm{am}} + \frac{8}{5}\right\} \\
& + S_{33}^{\mathrm{ao}}\left\{\frac{3}{35}F_{400}^{\mathrm{am}} - \frac{2}{7}F_{200}^{\mathrm{am}} + \frac{1}{5}\right\} + \frac{1}{8}(2S_{12}^{\mathrm{ao}} + S_{66}^{\mathrm{am}}) \\
& \times\left\{\frac{3}{35}F_{400}^{\mathrm{am}} + \frac{8}{21}F_{200}^{\mathrm{am}} + \frac{8}{5}\right\} + \frac{1}{2}(4S_{13}^{\mathrm{ao}} + S_{55}^{\mathrm{ao}} + S_{66}^{\mathrm{ao}}) \\
& \times\left\{-\frac{3}{35}F_{400}^{\mathrm{am}} - \frac{1}{21}F_{200}^{\mathrm{am}} + \frac{2}{15}\right\}
\end{aligned} \tag{22}$$

where the orientation factors in Eq. (21) may be given by

$$\begin{aligned}
& F_{200} = \tfrac{1}{2}(3\langle\cos^2\theta\rangle - 1), \qquad F_{202} = 3\langle\sin^2\theta\cos 2\eta\rangle, \\
& F_{400} = \tfrac{1}{8}(35\langle\cos^4\theta\rangle - 30\langle\cos^2\theta\rangle + 3), \\
& F_{402} = \tfrac{15}{2}\langle(7\cos^2\theta - 1)\sin^2\theta\cos 2\eta\rangle, \\
& F_{404} = 105\langle\sin^4\theta\cos 4\eta\rangle, \qquad G_{202} = 3\langle\sin^2\theta\sin 2\eta\rangle, \\
& G_{402} = \tfrac{1}{8}\langle(7\cos^2\theta - 1)\sin^2\theta\sin 2\eta\rangle, \\
& G_{404} = 105\langle\sin^4\theta\sin 4\eta\rangle.
\end{aligned} \tag{23}$$

The representation of Eq. (21) for a PVA crystal unit is much complicated in comparison with that of polyethylene. The problem that now arises has been how the value of the intrinsic compliances S_{uv}^{co} and S_{uv}^{ao} of PVA can be determined theoretically. The values as the pioneering work were obtained by Tashiro et al. [44] using a B matrix at absolute temperature. According to their paper, S_{uv}^{co} is given by

$$S_{uv}^{\mathrm{co}} = \begin{vmatrix} 6.87 & -3.98 & -0.03 & 0 & 0 & -5.04 \\ -3.98 & 10.90 & -0.08 & 0 & 0 & 0.73 \\ -0.03 & -0.08 & 0.35 & 0 & 0 & 0.07 \\ 0 & 0 & 0 & 9.28 & -0.68 & 0 \\ 0 & 0 & 0 & -0.68 & 61.05 & 0 \\ -5.04 & 0.73 & 0.07 & 0 & 0 & 27.6 \end{vmatrix} \times 10^{-12}\ \mathrm{cm^2/dyn}. \tag{24}$$

Because of the lack of inharmonic effects, the crystal lattice modulus, 282 GPa, in the chain direction given by $1/S_{33}^{\mathrm{co}}$ is much higher than the observed values (210–220 GPa) by X-ray diffraction at room temperature [45].

The intrinsic elastic compliance S_{uv}^{ao} of the amorphous phase needed in the numerical calculation is not quite certain. In accordance with the previous method [20,42], however, the values can be estimated as a crude approximation, assuming that the following relation between the potential energy $P(r)$ of Lennard-Jones and the atomic or

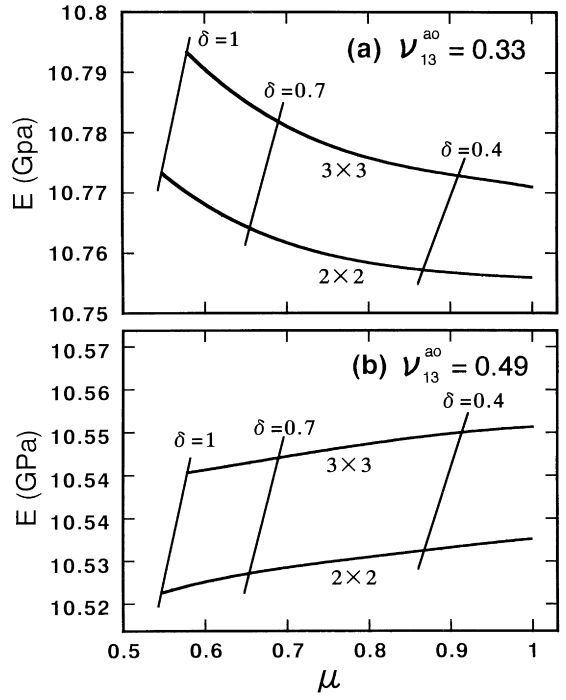

Fig. 13. The μ-dependence of Young's modulus calculated in Eqs. (13)–(27).

molecular distance r holds for a noncrystalline chain

$$P(r) = -\frac{c}{r^n} + \frac{d}{r^m} \tag{25}$$

where $m = 9$–12 and $n = 1$ or 6 for an ionic or molecular crystal, respectively. Then, neglecting the repulsion term in Eq. (25) for r greater than the equilibrium distance. The elastic compliance, S_{11}^{ao} and S_{22}^{ao}, may be estimated by taking the second-order derivative of $P(r)$ [42,46]. Then,

$$S_{11}^{ao} = S_{22}^{ao} = \left\{\frac{\rho_c}{\rho_a}\right\}^4 S_{11}^{c'} \tag{26}$$

where $S_{11}^{c'}$ correspond to S_{11}^{cv} at 0°. ρ_c and ρ_c are the intrinsic densities of the crystalline and amorphous phases, respectively. On the other hand, the expansion of the amorphous phase is assumed to occur only along the lateral direction of the polymer chain, not lengthwise. The compliance S_{33}^{ao} may be estimated by assuming that the modulus along the chain axis is proportional to the number of chain molecules in the unit area perpendicular to the chain direction, and that the modulus is independent of temperature [40,43]. Thus we have

$$S_{33}^{ao} = \left\{\frac{\rho_c}{\rho_a}\right\} S_{33}^{co}. \tag{27}$$

The other compliances are given by Hibi et al. [12]. In this paper, the Poisson ratios ν_{12}^{ao} $(= \nu_{13}^{ao})$ is an unknown parameter and is set to be 0.49 or 0.33. The former or latter value of ν_{12}^{ao} is selected in the case where the mechanical property of the amorphous phase is similar to an ideal rubber elasticity or somewhat tougher or glass state, respectively.

To calculate the mechanical properties according to the previous methods [12,20,42], the fourth-order orientation factor F_{400}^{am} of the amorphous chain segments must be estimated. Unfortunately, this factor cannot be obtained from birefringence measurements and therefore must be calculated by assuming a common function as an orientation function of amorphous chain segments. In this paper, the mean fourth power of direction $\langle\cos^4\theta\rangle_{am}$ was calculated from an inversely superposed Gaussian function given in a previous papers [20].

Fig. 13 shows the μ-dependence of Young's modulus E calculated at ν_{12}^{ao} $(= \nu_{13}^{ao}) = 0.33$ and 0.49. Here δ is determined automatically by $X_c = \mu^2\delta$ (X_c is volume crystallinity). The numerical calculation was carried out from Eqs. (15)–(27) using the intrinsic crystal elastic compliance S_{uv}^{co} proposed by Tashiro et al. [44]. These calculated values at $\lambda = 2\times2$ and 3×3 are hardly affected by Poisson's ratio of ν_{12}^{ao} $(= \nu_{13}^{ao})$ of the amorphous phases. E decreases slightly with μ, when ν_{12}^{ao} $(= \nu_{13}^{ao})$ is fixed to be 0.33. In contrast, E increases slightly with μ, when ν_{12}^{ao} $(= \nu_{13}^{ao})$ is fixed to be 0.49. This tendency predicts that even for two specimens with the same crystallinity and degree of molecular orientation, their Young's moduli slightly differ, depending on the composite mode of the crystalline and amorphous phases. However, the change is very small to be negligible.

It is seen that in spite of various composite modes by the change of μ, all the theoretical Young's moduli calculated using S_{uv}^{co} of Tashiro et al. [44] are in poor agreement with the experimental value, 2.89 GPa at $\lambda = 2\times2$ and 4.29 GPa at $\lambda = 3\times3$ in Table 1. Such large deviation is attributed to the comparison between the results measured at room temperature and the theoretical results at absolute temperature. Although the experimental values of Young's modulus is sensitive to the draw ratio, the theoretical values are less sensitive to the draw ratio as shown in Fig. 13 in comparison with the experimental values. This is thought to be due to the fact that the exact mechanical property of the simultaneous biaxially stretched PVA films by using a polycrystalline aggregate model cannot be represented by the theory for infinitesimal deformation of an anisotropic elastic body using 36 independent elastic compliances based on the homogeneous stress hypothesis. Another possibility is due to the fact that although the elastic compliance, S_{11}^{ao} and S_{33}^{ao}, depend on the molecular orientational degree of the amorphous chain segments, the values of S_{11}^{ao} and S_{33}^{ao} calculated by Eqs. (26) and (27) is related to the intrinsic values of the amorphous phase at the absolute temperature. If the real theoretical values of S_{uv}^{co} and S_{uv}^{ao} at room temperature are proposed, theoretical values are in good agreement with experimental values.

Here, we shall discuss the ultimate value of Young's modulus of an ideal simultaneous biaxially stretched film such that the crystallinity is 100% and the c-axes orient to the film surface perfectly. In this case, two cases can be

Table 3
Theoretical calculation of Young's modulus of ideal biaxially stretched films, in which crystallinity is 100% and the *c*-axes are oriented parallel to the film surface perfectly

	Case I[a]	Case II[b]
$\nu_{12}^{ao} (= \nu_{13}^{ao}) = 0.49$	13.43	13.34
$\nu_{12}^{ao} (= \nu_{13}^{ao}) = 0.33$	13.42	13.34

[a] Case I: preferential orientation of the (110) plane parallel to the film surface.
[b] Case II: random orientation of crystallites around the *c*-axis.

considered: (1) the *c*-axes and the (110) planes are oriented perfectly parallel to the film surface; (2) the *c*-axes are oriented perfectly parallel to the film surface but the crystallites rotate randomly around their own *c*-axis. In the former case, the generalized orientation factors can be obtained by substituting $\Phi_j = 53°$ into Eq. (23) instead of η and $\theta = 90°$, we obtain $F_{200} = -0.5$, $F_{202} = -0.826912$, $F_{400} = 0.375$, $F_{402} = 2.067280$, $F_{404} = -89.045050$, $G_{202} = 2.883785$, $G_{402} = -0.120157$ and $G_{404} = -55.641523$, while in the latter case, we obtain $F_{200} = -0.1$, $F_{202} = 0$, $F_{400} = 0.375$, $F_{402} = 0$, $F_{404} = 0$, $G_{202} = 0$, $G_{402} = 0$ and $G_{404} = 0$. In both of the cases X_c becomes unity.

Table 3 shows the results. The expected values are much lower than the ultimate value (200–220 GPa) corresponding to the crystal lattice modulus in the chain direction measured by X-ray diffraction [45]. This tendency is due to the fact that Young's modulus of a biaxially stretched film is isotropic on the film plane and consequently the value is sensitive to the compliance relating to shear modulus. In contrast, Young's modulus of a uniaxial film with a perfect molecular orientation depends on the compliance, S_{33}^{co}, in the chain direction directly. Accordingly, the ultimate value of Young's modulus of a simultaneous biaxially stretched film listed in Table 3 is less than 13.5 GPa at absolute temperature. This theoretical conclusion indicates the impossibility to prepare high-modulus and high-strength poly(vinyl alcohol) sheets.

Fig. 14 shows the CH resonance line for the 67.8-MHz CP/MAS and PST/MAS ^{13}C NMR spectra of the undrawn and drawn films with $\lambda = 3 \times 3$ measured at 36°C, respectively, and the corresponding results of the computer lineshape analysis of the total components of crystalline and amorphous phases. The CP/MAS spectra emphasize the contribution of the crystalline phase, while the PST/MAS spectra emphasize the contribution of the amorphous chain motion by NOE (nuclear Overhauser effect). According to previous works [47–50], the CH resonance line of each specimens splits into a triplet, I, II and III which are assigned to the central CH carbons I, II and III in *mm*, *mr* and *rr* sequences of the PVA chain with planar zigzag structure. Here, the OH group bonded to the CH carbon I forms intra-molecular hydrogen bonds with two OH groups on both sides in the *mm* sequence. On the other hand, the

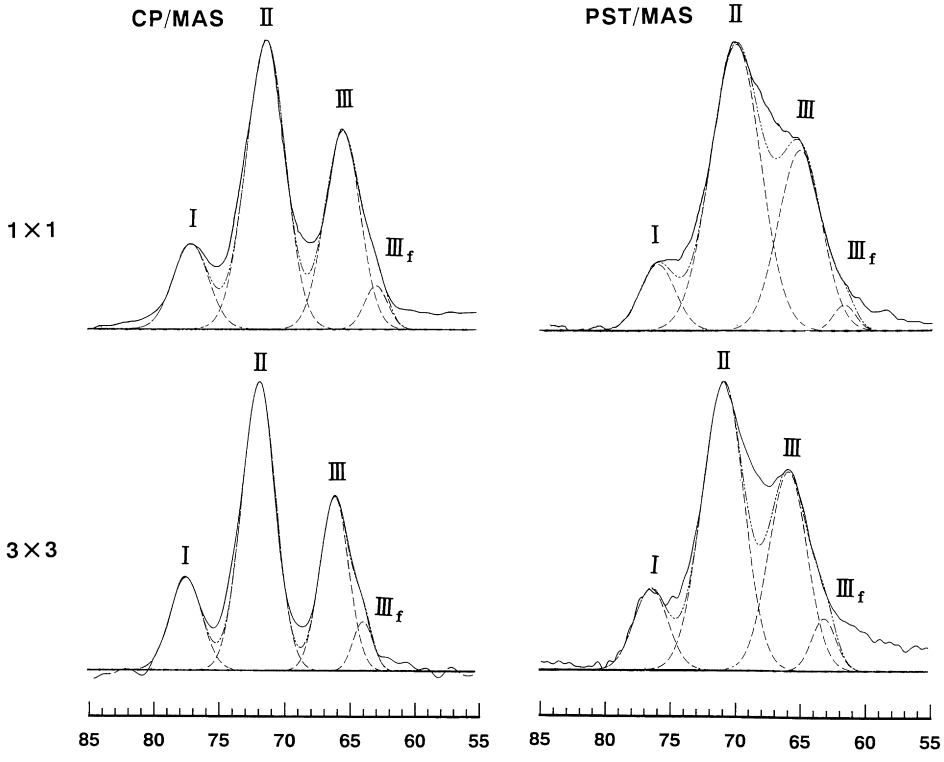

Fig. 14. Lineshape analysis for the CH line of CP/MAS and PST/MAS spectra measured for undrawn and drawn PVA films at 36°C. The broken line indicates the composite curves of the four components.

Table 4
Integrated fractions and linewidth of lines I, II and III of CH carbons obtained from the CP/MAS and PST/MAS spectra of undrawn and drawn (3 × 3) PVA dry gel films measured at 36 and 100°C

	Integrated fraction (%)				Linewidth (ppm)			
	I	II	III	III_f	I	II	III	III_f
At 36°C								
Undrawn (CP)	11.6	48.0	34.6	5.7	3.20	3.70	3.10	2.00
Drawn (CP)	12.7	48.2	33.8	5.3	3.05	3.60	3.20	2.20
Undrawn (PST)	9.3	45.2	44.3	1.2	3.20	4.50	4.50	2.00
Drawn (PST)	7.9	43.6	46.3	2.2	2.90	4.00	4.20	2.00
At 100°C								
Undrawn (CP)	13.6	50.4	31.5	4.5	3.20	3.50	3.20	2.10
Drawn (CP)	15.9	52.2	26.7	5.2	2.90	3.05	2.60	1.80
Undrawn (PST)	9.3	56.3	31.5	2.3	3.20	4.50	3.95	2.00
Drawn (PST)	11.6	50.8	32.3	5.3	3.10	3.80	3.50	2.20

corresponding OH groups associated with CH carbons II and III form one and no inter-molecular hydrogen bonds with the neighboring OH groups in *mr* and *rr* sequences, respectively. As shown in Fig. 14, an additional peak must be introduced upfield for line III as III_f. Each dashed line was assumed to be of Gaussian type and the composite curve of the three lines, I, II, III and III_f, which is represented by a dotted line, is in good agreement with the experimental spectrum. According to Horii et al. [50], the chemical shift of line III_f corresponds to that of the upfield line for the hydrated PVA. Based on IR spectroscopy [51], they pointed out that line III_f can be assigned to the CH carbons chemically bonded to the OH group, free from the intra- and inter-molecular hydrogen bonding and such a component may be detected as an upfield component of line III as a result of the enhancement in molecular mobility by water. The integrated fractions of lines I, II, III and III_f obtained by this analysis are given in Table 4 together with their linewidth. Furthermore, the measurements were also carried out at 100°C and the integrated faction and the linewidth are listed in Table 4.

As shown in Table 4, line I for the CP/MAS spectra at 36°C increases in intensity by elongation, while the intensity of line III is reduced. In contrast, the corresponding PST/MAS spectra show the inverse tendency. This suggests that in the crystalline phase, the inter-molecular hydrogen bonds may be broken by elongation and the intra-molecular hydrogen bonds are more preferably formed in the *mm* and *mr* sequences by elongation, while the inverse behavior occurs in the amorphous phase. The detailed observation reveals that the contribution from III_f in the PST/MAS spectra is much smaller than that in the CP/MAS spectra indicating that the number of OH group free from hydrogen bonds in the crystalline phase seems to be more than that in the amorphous phase.

In Table 4, the intensity of line I increases for both the CP/MAS and PST/MAS spectra at 100°C by elongation. In contrast, the intensity of line III in the CP/MAS spectra decreases but that in the PST/MAS spectrum increases. If the small increase of line III in the PST/MAS is within the arbitrary error on the curve fitting, the preferable formation in the *mm* and *mr* sequences by elongation becomes more pronounced in the crystalline and amorphous phases at elevated temperature. The present spectra, however, contain total contribution from crystalline and amorphous phases. To obtain the information of individual crystalline and amorphous phases, the separation from the total contribution of the CP/MAS spectra must be taken into consideration on the basis of spin–lattice relaxation time (T_1), by utilizing the difference of chain mobility between crystal and amorphous phases.

Fig. 15 shows the CH_2 resonance line at 36°C respectively and the corresponding results of the computer lineshape analysis, in which each dashed line was assumed to be of Gaussian type. Comparing the CP/MAS and PST/MAS spectra, much different effects are observed by elongation. The integrated fraction and linewidth measured at 100°C are also listed in Table 5. Through a series of the spectra, it is evident that peaks A and B are mainly attributed to the contribution from crystalline and amorphous regions, respectively. The analysis of the CP/MAS spectra in Table 5 indicates that the change of the linewidth is sensitive to the heating rather than the elongation, while the linewidth of the PST/MAS spectra is affected by both of the heating and elongation. At $\lambda = 1 \times 1$ (undrawn) and 3×3, the mass fraction of peak B in the PST/MAS spectra decreases in spite of an increase in temperature. This phenomenon is obviously due to an increase in crystallinity by annealing, as shown in Table 1. Judging from the linewidth and the mass fraction in a series of the spectra, it may be concluded that the disorder within crystallites decreased with temperature and consequently thermal and oriented crystallization was slightly developed. Especially, we must emphasize that the amorphous fraction decreases but the chain mobility becomes more active as temperature increases.

Returning to Fig. 5, the decreasing degree of the storage modulus in the temperature range of 35–100°C is less pronounced than that in the temperature range of −150 to 35°C. According to previous results [45], the crystal lattice modulus in the chain direction is independent of temperature and the decrease in Young's modulus in bulk with temperature is thought to be due to the drastic decrease of the modulus of the amorphous phase. In the present system, the storage modulus decreases with increasing temperature in the range of 35–100°C and the change in crystallinity was confirmed to be negligible by the preliminary experiments. Thus the decrease in the storage modulus is attributed to the decrease of modulus in the amorphous phase due to the active mobility of amorphous segments. Actually, the corresponding change of the linewidth of peak B in the PST/MAS spectra in Table 5 supports the drastic chain mobility in amorphous phase at elevated temperature.

Furthermore, the elastic compliance of the amorphous phase were given as a function of intrinsic crystal and amorphous densities in Eqs. (26) and (27) to calculate

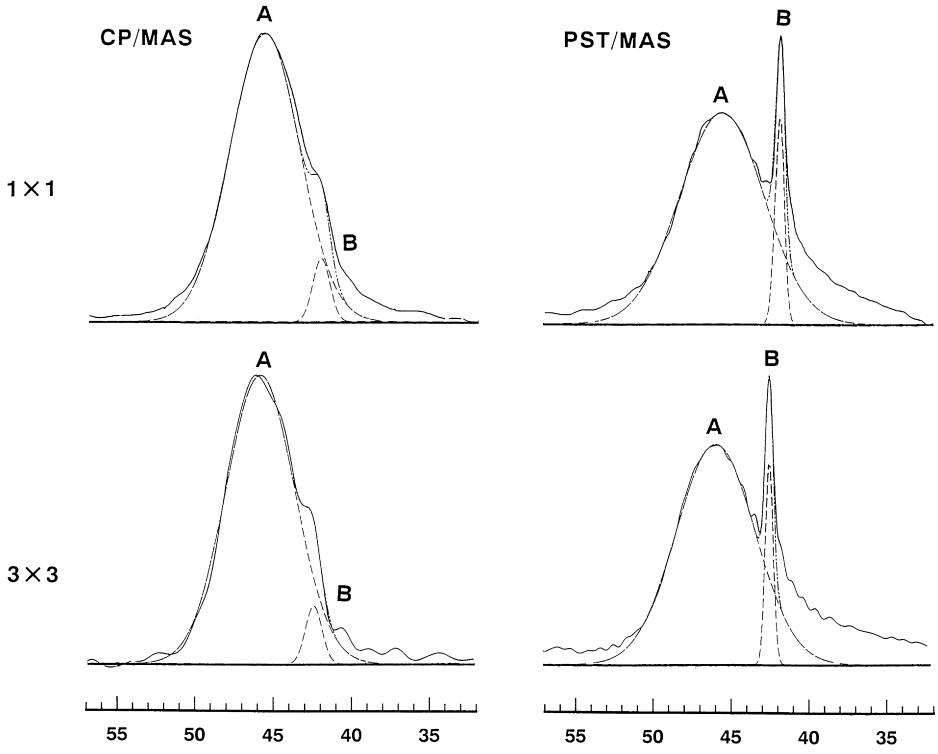

Fig. 15. Lineshape analysis for the CH_2 line of CP/MAS and PST/MAS spectra measured for undrawn and drawn PVA films at 36°C. The broken line indicates the composite curves of the two components.

Young's modulus in bulk. The two equations contain two big problems. One is a constant value of amorphous density independent of temperature and molecular orientational degree. The other one is the adoption of S_{ij}^{co} at absolute temperature. Here we must emphasize again that the amorphous density must be represented as a function of temperature and molecular orientational degree and the value of S_{uv}^{co} must be calculated by introducing inharmonic effects. Namely, the value of S_{11}^{ao} and S_{33}^{ao} must be given as a function of temperature in order to carry out the theoretical calculation of Young's modulus in bulk at elevated temperature. If the quantitative information concerning molecular mobility in the crystalline and amorphous phases can be derived from ^{13}C NMR, dramatic improvement shall be expected in the field of the mechanics of polymer materials. Actually, the modulus of the amorphous phase in PVA at room temperature is thought to be similar to that of the crystalline phase, since the increase in Young's modulus in bulk is very small in spite of the drastic increase in crystallinity in Table 1.

Table 5
Integrated fractions and linewidth of lines A and B of CH_2 carbons obtained from the CP/MAS and PST/MAS spectra of undrawn and drawn (3 × 3) PVA dry gel films measured at 36 and 100°C

	Integrated fraction (%)		Linewidth (ppm)	
	A	B	A	B
At 36°C				
Undrawn (CP)	93.9	6.1	5.85	1.30
Drawn (CP)	95.1	4.9	5.75	1.30
Undrawn (PST)	82.1	17.9	7.55	1.05
Drawn (PST)	89.0	11.0	7.15	1.00
At 100°C				
Undrawn (CP)	94.8	5.2	5.25	1.30
Drawn (CP)	95.4	4.6	5.20	1.25
Undrawn (PST)	90.4	9.6	6.40	0.70
Drawn (PST)	91.7	8.3	6.00	0.60

4. Conclusion

Simultaneous biaxial stretching was carried out by using PVA gel films which were prepared by crystallization from solutions. Swollen gels with large amount of solvents (80–90%) showed an X-type pattern under Hv polarization condition indicating the existence of rod-like textures, the optical axes being oriented parallel or perpendicular to the rod axis. The appearance of the optical anisotropic rods is attributed to the formation of ordering structure in a polymer-rich phase that arises due to the concentration fluctuation in the solution. The Hv pattern from gels with solvent content <80% shows a circular type indicating the formation of a random array of quasi-crystallites smaller than the wavelength of the incident beam. This is probably due to the appearance of small quasi-crystallites within the polymer-rich phase and the decrease in solvent content

enhances the progression of crystallization detected by X-ray diffraction. In this process the gels become stiffer. The repeated stress–strain curves for gels with 80% solvent content pass through almost the same route up to the 40th run. This means that very small quasi-crystallites within the gel play a significant role as cross-linked points to cause rubber elasticity.

Young's modulus of the biaxially stretched film were much lower than that of the uniaxially stretched film with almost the same draw ratio, although the crystallinity and melting point were also the same. To address the poor values of Young's modulus, theoretical analysis was carried out by using the generalized orientation factors of crystallites and amorphous chain segments on the basis of a two-phase model assuring the homogeneous stress hypothesis for a polycrystalline material. The experimental values at room temperature were less than half of the theoretical ones at absolute temperature. Such a large discrepancy is due to the fact that the intrinsic elastic compliance of a PVA crystal unit cell at absolute temperature was adopted to determine the compliance of amorphous phase, S_{11}^{ao} and S_{33}^{ao}, needed for the numerical calculation of Young's modulus. Accordingly, the large difference shall be solved, if the value of intrinsic elastic compliance of a PVA crystal unit at room temperature is proposed on the basis of the recent molecular dynamics and the amorphous density is given as a function of temperature on basis of ^{13}C NMR. Furthermore, the ultimate value of Young's modulus was estimated by assuming an ideal simultaneous biaxial stretching film with 100% crystallinity and the perfect orientation of the *c*-axes parallel to the film surface. The theoretical values were less than 13.5 GPa even at absolute temperature. This means it is difficulty to produce high-modulus and high-strength PVA sheets. Even so, the theoretical values indicates the possibility to produce PVA sheets whose Young's modulus is higher than that of polyethylene with further improvement of techniques of more significant drawing PVA films.

References

[1] Smith P, Lemstra PJ, Kalb B, Pennings AJ. Polym Bull 1979;1:733.
[2] Smith P, Lemstra PJ. J Mater Sci 1980;15:505.
[3] Smith P, Lemstra PJ, Pippers JPL, Kiel AM. Colloid Polym Sci 1981;258:1070.
[4] Smith P, Lemstra PJ. J Polym Sci, Polym Phys Ed 1981;19:1007.
[5] Smith P, Lemstra PJ, Booij HC. J Polym Sci, Polym Phys Ed 1981;19:877.
[6] Matsuo M, Sawatari C. Macromolecules 1986;19:2036.
[7] Ogita T, Yamamoto R, Suzuki N, Ozaki F, Matsuo M. Polymer 1991;32:822.
[8] Sakurada I, Nukushina Y, Ito T. J Polym Sci 1962;57:651.
[9] Kavesh S, Prevorsek DC. Int J Polym Mater 1995;30:15.
[10] Sakaguchi N, Oda T, Nakai A, Kawai H. Sen-i Gakkaishi 1977;33:499.
[11] Takahara H, Kawai H, Yamaguchi Y, Fukushima A. Sen-i Gakkaishi 1969;25:60.
[12] Hibi S, Maeda M, Mizuno M, Nomura S, Kawai H. Sen-i Gakkaishi 1973;29:152.
[13] Sakai Y, Miyasaka K. Polymer 1988;29:1608.
[14] Sakai Y, Miyasaka K. Polymer 1990;31:51.
[15] Sakai Y, Uematsu K, Miyasaka K. Polymer 1993;34:318.
[16] Gerrits NSJA, Young RJ, Lemstra PJ. Polymer 1990;31:231.
[17] Gerrits NSJA, Lemstra PJ. Polymer 1991;32:1770.
[18] Gerrits NSJA, Young RJ. J Polym Sci, Part B: Polym Phys 1991; 29:825.
[19] Bastiaansen CWM, Leblans PJR, Smith P. Macromolecules 1990; 23:2365.
[20] Nakashima T, Xu C, Bin Y, Matsuo M. Submitted for publication.
[21] Roe RJ, Krigbaum WR. J Chem Phys 1964;40:2608.
[22] Krigbaum WR, Roe RJ. J Chem Phys 1964;41:737.
[23] Roe RJ. J Appl Phys 1965;36:2024.
[24] Cha WI, Hyon SH, Ikada Y. J Polym Sci, Part B: Polym Phys 1994; 32:297.
[25] Sakurada I, Nukushina K, Sone Y. Kobunshi Kagaku 1955;12:506.
[26] Matsuo M, Sawatari C, Ohhata T. Macromolecules 1988;21:1317.
[27] Matsuo M, Sato R, Yanagida N, Shimizu Y. Polymer 1992;33:1640.
[28] Matsuo M, Kawase M, Sugiura Y, Takematsu S, Hara C. Macromolecules 1993;26:4461.
[29] Rhodes M, Stein RS. J Polym Sci, Part A-2 1969;7:1539.
[30] Matsuo M, Sugiura Y, Takematsu S, Ogita T, Sakabe T, Nakamura R. Polymer 1997;38:5953.
[31] Sawatari C, Okumura T, Matsuo M. Polym J 1986;18:741.
[32] Sawatari C, Matsuo M. Macromolecules 1989;22:2968.
[33] Khanna YP, Turi EA, Taylor TJ, Vickroy VV, Abott RF. Macromolecules 1985;18:1302.
[34] Kawai H, Suehiro S, Kyu T, Shimomura A. Polym Engng Rev 1983;3:109.
[35] Spendly W, Hext GR, Himsworth FR. Technometrics 1962;4:441.
[36] Stein RS, Norris FH. J Polym Sci 1956;21:381.
[37] Nomura S, Kawai H. J Polym Sci, Part A-2 1966;4:797.
[38] Clement C, Botherel P. C. R. Acad Sci (Paris) 1964;258:4757.
[39] Nitta I, Taguchi I, Chatani Y. Ann Rep Inst Fiber Sci, Osaka Univ 1957;10:1.
[40] Bunn CW, de Daubeny RP. Trans Faraday Soc 1954;50:1173.
[41] Matsuo M. Macromolecules 1990;23:326.
[42] Matsuo M, Sawatari C, Iwai Y, Ozaki F. Macromolecules 1990;23:3266.
[43] Sawatari C, Matsuo M. Macromolecules 1986;19:2726.
[44] Tashiro K, Kobayashi M, Tadokoro H. Macromolecules 1978;11:914.
[45] Matsuo M, Harashina Y, Ogita T. Polym J 1993;25:319.
[46] Nomura S, Kawabata S, Kawai H, Yamaguchi Y, Fukushima A, Takahara H. J Polym Sci, Part A-2 1969;7:325.
[47] Terao T, Maeda S, Saika A. Macromolecules 1983;16:1535.
[48] Inoue Y, Chujo R, Nishioka A, Nozakura S, Iimuro H. Polym J 1973; 4:266.
[49] Wu TK, Sheer ML. Macromolecules 1977;10:529.
[50] Horii F, Hu S, Ito T, Odani H, Kitamaru R, Matsuzawa S, Yamaura K. Polymer 1992;33:2299.
[51] Akahane T, Kazuya Y, Nakayasu H. Kobunshi Ronbunshu 1980;37:383.